ELSEVIER

International Journal of Heat and Fluid Flow 19 (1998) 338–347

International Journal of HEAT AND FLUID FLOW

# Scaling of the turbulent boundary layer along a flat plate according to different turbulence models

R.A.W.M. Henkes [1]

*J.M. Burgers Centre for Fluid Mechanics, and Faculty of Aerospace Engineering, Delft University of Technology, Kluyverweg 12629 HS Delft, The Netherlands*

Received 30 November 1996; accepted 8 March 1998

**Abstract**

At sufficiently large Reynolds number the turbulent boundary layer along a flat plate under zero pressure gradient can be split up in an inner and outer layer. The classical theory says that a law-of-the-wall holds in the inner layer, and a defect law in the outer layer. It is shown that four different types of commonly used turbulence models (an algebraic, $k$–$\epsilon$, $k$–$\omega$ and a differential Reynolds-stress model) all reproduce the classical similarity scalings for $\mathrm{Re}_\theta$ above about $10^4$. This was verified by numerically solving the turbulent boundary-layer equations for Reynolds numbers (based on the momentum-loss thickness) in between 300 and $5 \times 10^7$. The boundary-layer solution in the outer layer is shown to converge to the similarity solution of a defect-layer equation. All turbulence models considered give a wall function and defect law that is close to Direct Numerical Simulations of Spalart (1988) and new high-Reynolds-number experiments by Fernholz et al. (1995). An exception is the algebraic model that gives a too thin boundary layer. 

*Keywords:* Turbulent boundary layer; Law of the wall; Defect law

## Notation

| | |
|---|---|
| $c_f$ | wall-shear coefficient $(= \tau_\omega/(\frac{1}{2}\rho U^2) = 2(u_\tau/U)^2)$ |
| $c_\mu$ | constant in the expression for the turbulent viscosity in the $k$–$\epsilon$ model |
| $C$, $C'$ | coefficients in the logarithmic wall function for the velocity |
| $C^*$ | parameter for the outer layer $(= \int_0^\infty f^2 \,\mathrm{d}\eta = G)$ |
| $f$ | defect law for the velocity, Eq. (3) |
| $F$ | wall function, Eq. (12) |
| $G$ | Clauser parameter $(= \int_0^\infty ((U-u)/u_\tau)^2 \,\mathrm{d}(y/\Delta))$ |
| $H$ | shape factor $(= \delta^*/\theta)$ |
| $k$ | turbulent kinetic energy |
| $r$ | defect law for the Reynolds shear stress, Eq. (3) |
| $R_\mathrm{o}$ | squared velocity scale in the outer layer |
| $\mathrm{Re}_x$ | $x$-based Reynolds number $(= Ux/\nu)$ |
| $\mathrm{Re}_x$ | $\theta$-based Reynolds number $(= U\theta/\nu)$ |
| $u$ | velocity component in $x$ direction |
| $u_\tau$ | wall-shear stress velocity $(= (\tau_\omega/\rho)^{1/2})$ |
| $U$ | free-stream velocity |
| $U_\mathrm{o}$ | velocity scale in the outer layer |
| $v$ | velocity component in $y$ direction |
| $x$ | coordinate along the plate |
| $y$ | coordinate normal to the plate |

*Greek*

| | |
|---|---|
| $\alpha$ | coefficient in the defect-layer equation (6) |
| $\alpha_1$,$\alpha_2$ | coefficients in the stretching function for the numerical grid points |
| $\gamma$ | coefficient in defect-layer equation (6) |
| $\delta$ | length scale in the outer layer |
| $\tilde{\delta}$ | length scale in Coles' defect law, Eqs. (25) and (26) |
| $\delta^*$ | displacement thickness $\left(= \int_0^\infty (1-u/U)\,\mathrm{d}y\right)$ |
| $\Delta$ | Clauser–Rotta length scale for the outer layer $(= \delta^* U/u_\tau)$ |
| $\Delta^*$ | parameter in the outer layer, see Eq. (29) |
| $\epsilon$ | turbulent dissipation rate |
| $\eta$ | scaled $y$ coordinate in the outer layer $(= y/\delta)$ |
| $\theta$ | momentum-loss thickness $(= \int_0^\infty (u/U)(1-u/U)\,\mathrm{d}y)$ |
| $\kappa$ | Von Kármán constant |
| $\mu$ | dynamic viscosity |
| $\nu$ | kinematic viscosity |
| $\nu_t$ | turbulent viscosity |
| $\chi$ | coefficient in defect-layer equation (6) |
| $\xi$ | $= x$ |
| $\Pi$ | Coles' wake-strength parameter |
| $\rho$ | density |
| $\tau_\mathrm{w}$ | wall-shear stress $(= \mu(\partial u/\partial y)_\mathrm{w})$ |
| $\omega$ | quantity proportional to $\epsilon/k$ in the $k$–$\omega$ model; also coefficient in the defect-layer equation (6); also wake function, Eq. (25) |

[1] Address for correspondence: Fluid Flow and Thermodynamics (OGBE/6), Shell International Oil Products B.V., Badhuisweg 3, 1031 CM Amsterdam, The Netherlands. E-mail: Ruud.A.W.Henkes@opc.shell.com.

0142-727X/98/$19.00 
PII: S0142-727X(98)10009-7

*Superscripts*

+ quantity in wall units, i.e. scaled with the velocity $u_\tau$ and length $\nu/u_\tau$

′ turbulent fluctuation

*Subscripts*

o quantity in the outer layer

w quantity at the wall

## 1. Introduction

There still is a debate in the literature on the proper scalings of the turbulent boundary layer along a plate with or without streamwise pressure gradient. Knowledge of the scalings is not only important for a better understanding of the fundamentals of turbulence, but it can also tell how the experiments for scale models in the wind tunnel can be extrapolated to the full scale conditions. In the present study the scalings are derived for the turbulent boundary layer in a zero pressure gradient, as dictated by four commonly used turbulence models, namely an algebraic model, $k$–$\epsilon$ model, $k$–$\omega$ model and a differential Reynolds-stress model. The scalings are derived from the straightforward numerical solution of the boundary-layer equations. Computations are made up to the very large Reynolds number of $\mathrm{Re}_x = 10^{11}$ ($\mathrm{Re}_\theta \approx 5 \times 10^7$), which is sufficient for the similarity scalings to appear.

The classical theory finds that the boundary layer can be split up in an inner layer (wall function), with the velocity scale $u_\tau$ and the length scale $\nu/u_\tau$, and an outer layer (defect layer), with the velocity scale $u_\tau$ and the length scale $\Delta = \delta^*(U/u_\tau)$ (where $U$ denotes the local free-stream velocity). For large $y^+$ the theory predicts the logarithmic shape of the wall function. Furthermore $u_\tau/U \to 0$ for $\mathrm{Re}_\theta \to 0$. Recently George et al. (1992) have doubted the correctness of the classical theory, and instead they propose a power-law dependence for the wall function and a nonzero constant for $U/u_\tau$ at large Reynolds number. Barenblatt (1993) has shown, particularly for the fully developed pipe flow, that the scalings depend on the assumptions made; besides the classical logarithmic scaling law of the wall also a power-law expression can be derived.

Tennekes and Lumley (1972) and Wilcox (1993) have derived a defect-layer equation, that describes the similarity solution in the outer layer. This equation is obtained by transforming the boundary-layer equations with the help of the classical outer-layer scalings.

The aims of this paper are to

- Find the proper scalings in the inner and outer layer according to commonly used turbulence models.
- Verify whether the solution in the defect-layer as predicted by the boundary-layer equations is indeed described by the defect-layer equation proposed by Tennekes and Lumley and by Wilcox.
- Compare the performance of the different turbulence models in the inner and outer layer at large Reynolds number with recent Direct Numerical Simulations of Spalart (1988) and with new experimental data due to Fernholz et al. (1995).
- Show (by combining turbulence models, DNS, and experiments) that the classical scalings seem to correctly cover the physics of a turbulent boundary layer under zero streamwise pressure gradient.

It is emphasized that the present study cannot prove that the classical scalings are correct, because turbulence models are based on underlying assumptions. This study provides a consistent way to derive the scalings for a given turbulence model. If future studies will support that the classical scalings need modification (e.g. according to the theory of George et al. or Barenblatt) the same approach can be followed to update the turbulent models such that the modified scalings are reproduced.

## 2. Boundary-layer equations

In this section a short overview is given of existing knowledge on the scalings of the turbulent boundary layer along a flat plate.

For the incompressible boundary layer along a plate with zero streamwise pressure gradient, the Reynolds-averaged Navier–Stokes equations can be simplified to the turbulent boundary-layer equations:

$$\frac{\partial u}{\partial x} + \frac{\partial v}{\partial y} = 0, \tag{1}$$

$$u\frac{\partial u}{\partial x} + v\frac{\partial u}{\partial y} = \nu\frac{\partial^2 u}{\partial y^2} - \frac{\partial}{\partial y}\overline{u'v'}. \tag{2}$$

The boundary layer can be split up in an outer layer and an inner layer, as described below. Both layers are defined by their own specific scalings, which appear for increasingly large local Reynolds number. Mainly based on physical arguments, the classical scalings for the turbulent boundary layer in a zero pressure gradient were derived by different scientists, including Von Kármán (1930), Millikan (1938), Rotta (1950), Clauser (1954), and Coles (1956).

A similarity solution exists in the outer layer, if the velocity and turbulence profiles can be scaled with a single velocity scale $U_\mathrm{o}$ and length scale $\delta$ in such a way that the scaled solution becomes independent of the $x$ coordinate, i.e.

$$\frac{U-u}{U_\mathrm{o}} = f\left(\frac{y}{\delta}\right) \quad \text{and} \quad \frac{\overline{-u'v'}}{R_\mathrm{o}} = r\left(\frac{y}{\delta}\right), \tag{3}$$

$R_\mathrm{o}$ will turn out to be proportional to $U_\mathrm{o}^2$. Under the assumption that molecular diffusion can be neglected in the outer layer, transformation of Eq. (2) with $\xi = x$ and $\eta = y/\delta$ gives

$$\left[-\frac{U}{U_\mathrm{o}}\frac{\delta}{U_\mathrm{o}}\frac{\mathrm{d}U_\mathrm{o}}{\mathrm{d}\xi}\right]f + \left[\frac{\delta}{U_\mathrm{o}}\frac{\mathrm{d}U_\mathrm{o}}{\mathrm{d}\xi}\right]f^2 + \left[\frac{U}{U_\mathrm{o}}\frac{\mathrm{d}\delta}{\mathrm{d}\xi}\right]\eta f' + \left[-\frac{\mathrm{d}\delta}{\mathrm{d}\xi} - \frac{\delta}{U_\mathrm{o}}\frac{\mathrm{d}U_\mathrm{o}}{\mathrm{d}\xi}\right]f'\int_0^\eta f\,\mathrm{d}\eta = \frac{R_\mathrm{o}}{U_\mathrm{o}^2}r', \tag{4}$$

where a prime denotes differentiation to $\eta$. For complete similarity of this equation, all contributions in the terms between brackets must be proportional to each other. As a consequence $U_\mathrm{o} \propto U$, which does *not* agree with the classical theory of the law-of-the-wake theory where $U_\mathrm{o} \propto u_\tau$. As shown by Townsend (1976) and by George et al. (1992), if also the equations for the turbulence admit complete similarity, it follows that $U_\mathrm{o} \propto u_\tau \propto U$, and that $\delta \propto \delta^* \propto \theta \propto x - x_0$ (here $x_0$ is a virtual origin). Furthermore the velocity in the inertial sublayer (i.e. the overlapping region between the inner and the outer layer) will then show a power-law dependence on the wall coordinate. George et al. expect that these properties will indeed show up for sufficiently large Reynolds numbers, i.e. for $\mathrm{Re}_\theta$ above $10^5$ (with $\mathrm{Re}_\theta = U\theta/\nu$, and $\theta$ is the momentum-loss thickness). An argument against the proposal by Townsend and George et al. is that the restriction that all terms between brackets must be proportional to each other is too strong; the vanishing of terms between brackets for increasing Reynolds numbers is also consistent. This latter restriction enables the classical scalings to define a similarity solution.

Indeed experiments, which only exist for Reynolds numbers up to about $\mathrm{Re}_\theta = 10^5$, seem to support that the classical theory is valid; an overview is given be Dussauge et al. (1996). The classical scalings are

$$U_o = u_\tau, \qquad \delta = \delta^* \frac{U}{u_\tau}, \qquad R_o = u_\tau^2. \tag{5}$$

Substituting these scalings into Eq. (4) gives the following defect-layer equation,

$$-2\omega f + \gamma f^2 + (\alpha - 2\omega)\eta f' - \chi f' \int_0^\eta f \, \mathrm{d}\eta = r', \tag{6}$$

with

$$\alpha = \left(\frac{U}{u_\tau}\right)^2 \frac{\mathrm{d}\delta^*}{\mathrm{d}\xi}, \qquad \omega = \frac{1}{2}\frac{\delta^*}{u_\tau}\left(\frac{U}{u_\tau}\right)^2 \frac{\mathrm{d}u_\tau}{\mathrm{d}\xi},$$
$$\gamma = \frac{U}{u_\tau}\frac{\delta^*}{u_\tau}\frac{\mathrm{d}u_\tau}{\mathrm{d}\xi}, \qquad \chi = \frac{U}{u_\tau}\frac{\mathrm{d}\delta^*}{\mathrm{d}\xi}. \tag{7}$$

As shown by Wilcox (1993), an additional expression for $\alpha$ can be derived by considering the integral momentum equation

$$\frac{\mathrm{d}\theta}{\mathrm{d}x} = \frac{c_f}{2}, \tag{8}$$

where the wall-shear stress coefficient is defined as $c_f = \tau_w/(\frac{1}{2}\rho U^2) = 2(U_\tau/U)^2$ (and $\tau_w = \mu(\partial u/\partial y)_w$). Using Eq. (7), relation (8) can also be written as

$$\alpha\frac{\mathrm{d}\theta}{\mathrm{d}x} = \frac{\mathrm{d}\delta^*}{\mathrm{d}x}. \tag{9}$$

To find the limiting value for the shape factor $H(=\delta^*/\theta)$ for increasing Reynolds number, we first substitute the scalings (5) in the common definitions for $\delta^*$ and $\theta$. The definition of $\delta^*$ leads to the integral restriction

$$\int_0^\infty f \, \mathrm{d}\eta = 1. \tag{10}$$

The definition of $\theta$ leads to

$$\frac{1}{H} = \frac{\theta}{\delta^*} = 1 - C^*\frac{u_\tau}{U} \quad \text{with} \quad C^* = \int_0^\infty f^2 \, \mathrm{d}\eta. \tag{11}$$

As $u_\tau/U \to 0$ for $\mathrm{Re}_x \to \infty$, this relation shows that $H \to 1$ for very large Reynolds numbers. Substituting $H = 1$ in Eq. (9) gives $\alpha = 1$.

Approaching the wall, the similarity solution in the outer layer must match with the wall function in the inner layer. Under the assumption that convection can be neglected close to the wall, the boundary-layer equations give the well-known wall function for the velocity,

$$u^+ = F(y^+), \tag{12}$$

where the + superscript is used to denote that the quantities are non-dimensionalized with inner-layer scalings (i.e. the velocity scale $u_\tau$ and the length scale $\nu/u_\tau$). The equations in the inner layer also give for the Reynolds-shear stress:

$$\lim_{y^+\to\infty} \overline{-u'v'}^{\,+} = 1. \tag{13}$$

Using the theory of matched asymptotic expansions, Millikan (1938) has proposed that an overlapping region, i.e. the inertial sublayer, can exist in between the outer layer (for $\eta \to 0$) and the inner layer (for $y^+ \to \infty$), where both the defect law and the law-of-the-wall hold. This gives

$$\lim_{y^+\to\infty} u^+ = F(y^+) = \frac{1}{\kappa}\ln(y^+) + C \tag{14}$$

and

$$\lim_{\eta\to 0} \frac{U-u}{u_\tau} = f(\eta) = -\frac{1}{\kappa}\ln(\eta) + C'. \tag{15}$$

The last term gives a boundary condition for the defect-layer equation at $\eta \to 0$.

To find the wall-shear stress law, $u$ can be eliminated from Eqs. (14) and (15), which gives

$$c_f = 2\left(\frac{u_\tau}{U}\right)^2 = \frac{2}{[C + C' + (1/\kappa)\ln \mathrm{Re}_{\delta^*}]^2}, \tag{16}$$

with $\mathrm{Re}_{\delta^*} = U\delta^*/\nu$.

Substitution of Eq. (16) into Eq. (7), and applying Eqs. (9) and (11) gives the following asymptotic expressions for the coefficients in Eq. (6),

$$\frac{1}{\alpha} = \frac{1}{H} = 1 - C^*\frac{u_\tau}{U}, \qquad \omega = -\frac{1}{2\kappa}\frac{u_\tau}{U},$$
$$\gamma = -\frac{1}{\kappa}\left(\frac{u_\tau}{U}\right)^2, \qquad \chi = \frac{u_\tau}{U}. \tag{17}$$

Because $u_\tau/U \to 0$ for $\mathrm{Re}_\theta \to \infty$ (see Eq. (16)), substitution of the asymptotic values of the coefficients (17) into (16) gives the defect-layer equation:

$$\eta f' = r', \tag{18}$$

with boundary conditions

$$f \to -\frac{1}{\kappa}\ln\eta + C' \quad \text{for} \quad \eta \to 0,$$
$$f \to 0 \quad \text{for} \quad \eta \to \infty,$$

and the integral restriction $\int_0^\infty f \, \mathrm{d}\eta = 1$.

### 2.1. Turbulence models

To solve the equations, a turbulence model is needed to represent the Reynolds shear stress, i.e. $\overline{u'v'}$ in the boundary-layer Eq. (2), or $r$ in the defect-layer equation (18). The following four turbulence models were considered.

- Algebraic model of Cebeci and Smith (1974).
- Two-equation low-Reynolds-number $k$–$\epsilon$ model of Launder and Sharma (1974).
- Two-equation low-Reynolds-number $k$–$\omega$ model of Wilcox (1993).
- Differential Reynolds-stress model of Hanjalić et al. (1995) (see also Jakirlić et al., 1994).

For the precise formulation of the different models the reader is referred to the originals papers, or to Henkes (1997). The algebraic model and the two-equation models approximate the turbulence through a turbulent viscosity, which is defined as

$$\overline{-u'v'} = \nu_t \frac{\partial u}{\partial y}. \tag{19}$$

The algebraic model couples $\nu_t$ to the velocity via an algebraic relation; the $k$–$\epsilon$ model solves differential equations for the turbulent kinetic energy $k$ and the turbulent dissipation rate $\epsilon$, as appearing in $\nu_t = c_\mu k^2/\epsilon$ (with $c_\mu$ is a constant); the $k$–$\omega$ model solves differential equations for $k$ and $\omega$ ($\propto \epsilon/k$), as appearing in $\nu_t = \alpha^* k/\omega$ (where $\alpha^*$ is a dimensionless function); and the Differential Reynolds-Stress Model (DRSM) solves a differential equation for the Reynolds shear stress $\overline{u'v'}$ itself (and for the three Reynolds normal stresses), as well as a differential equation for $\epsilon$.

All these four models have in common that the logarithmic part of the wall-function for the velocity is already captured in the model, i.e. the turbulence model is such that (14) is the solution of the boundary-layer equations for large $y^+$. This can be checked by neglecting the convection in the differential

equations for the turbulence model and taking the limit $y^+ \to \infty$. This gives for the inertial sublayer:

$$u^+ = \frac{1}{\kappa}\ln\, y^+ + C, \qquad k^+ = \frac{1}{c_\mu^{1/2}},$$
$$\epsilon^+ = \frac{1}{\kappa y^+}, \qquad \nu_t^+ = \kappa y^+, \qquad \overline{-u'v'}^+ = 1. \tag{20}$$

### 2.2. Numerical treatment

In order to find numerical solutions, the boundary-layer equations (1) and (2), with the specific turbulence models, are discretized with a second-order accurate finite-difference scheme on a Cartesian grid. The numerical code has been developed in-house, and more details are given by Henkes (1990). The calculation was started at $\mathrm{Re}_\theta = 300$, by prescribing the profiles obtained from Direct Numerical Simulations (DNS) by Spalart (1988) as initial solution. The computations were extended in streamwise direction up to about $\mathrm{Re}_\theta = 5 \times 10^7$ (which is equivalent to $\mathrm{Re}_x = 10^{11}$).

As the boundary layer is growing for increasing Reynolds number, whereas the inner layer becomes thinner compared to the boundary layer thickness, at several $x$ stations the outer edge of the computational domain was increased and the $y$ grid points were redistributed. To achieve that sufficient grid points are positioned in the inner layer very close to the wall a very efficient stretching function was used, reading

$$\frac{y_j}{y_{j\max}} = 1 + \frac{\tanh[\alpha_1(j/j\max - 1)/2]}{\tanh(\alpha_1/2)},$$
$$j = 0, 1, \ldots, j\max, \tag{21}$$

where $j$ max is the maximum number of grid point across the boundary-layer thickness. The coefficient $\alpha_1$ is derived from the expression $\alpha_2 = \alpha_1/\sinh(\alpha_1)$, in which $\alpha_2$ is chosen close to zero; the smaller $\alpha_2$, the stronger the relative grid refinement along the wall. The chosen outer edge of the boundary layer was checked to be sufficiently large to have a negligible effect on the solution. A typical calculation was split up in four parts in $x$-direction, and each part was computed with $2000 \times 200$ grid points. Doubling the number of grid points in both directions was applied to check that the results are numerically accurate. Therefore all results presented in this paper were verified to have a very small numerical error, both in the inner layer and the outer layer, even at the highest Reynolds numbers presented.

Also the defect-layer equation (18), including corresponding equations for the turbulence model, was numerically solved. The derivatives were discretized with finite differences. 200 grid points were used in $\eta$ direction, which was checked to be sufficient by doubling the number of grid points.

### 2.3. Characteristic parameters

A characteristic integral thickness for the boundary layer is

$$\Delta = \int_0^\infty \frac{U-u}{u_\tau}\,\mathrm{d}y. \tag{22}$$

Dussauge et al. (1996) refer to this quantity as the Clauser–Rotta thickness. It equals the proper length scale of the outer layer, i.e.

$$\delta = \Delta = \frac{\delta^* U}{u_\tau}. \tag{23}$$

A parameter that can be used to monitor whether similarity in the outer layer has been established is the so-called Clauser parameter, which is defined as

$$G = \int_0^\infty \left(\frac{U-u}{u_\tau}\right)^2 \mathrm{d}\left(\frac{y}{\Delta}\right) = \frac{1 - 1/H}{(c_f/2)^{1/2}}. \tag{24}$$

Comparison with Eq. (11) shows that $G = C^*$.

Coles (1956) has proposed to write the velocity in the outer layer as

$$\frac{u}{u_\tau} = \frac{1}{\kappa}\ln(y^+) + C + \frac{\Pi}{\kappa}\omega\left(\frac{y}{\tilde{\delta}}\right). \tag{25}$$

In fact this is the logarithmic wall function plus a correction term. On grounds of experiments Coles found that the function $\omega$ is a universal function, independent of the streamwise pressure gradient, but $\Pi$ can depend on $x$. The function $\omega$ is also referred to as the wake function, and it defines the law-of-the-wake. For small $y/\tilde{\delta}$ the logarithmic wall function should be retained, which defines the boundary condition $\omega(0) = 0$. Coles has defined $\tilde{\delta}$ by $\int_0^\delta \omega(y/\tilde{\delta}) = 1$; at the outer edge $y = \tilde{\delta}$ the arbitrary boundary condition $\omega(1) = 2$ is taken (another choice only changes the level of $\Pi$). Using $u = U$ at $y = \tilde{\delta}$, Coles could rewrite Eq. (25) as the defect law

$$\frac{U-u}{u_\tau} = -\frac{1}{\kappa}\ln\left(\frac{y}{\tilde{\delta}}\right) + \frac{\Pi}{\kappa}\left(2 - \omega\left(\frac{y}{\tilde{\delta}}\right)\right). \tag{26}$$

Using the definition of $\delta^*$, under the assumption that Eq. (25) holds for whole the boundary layer thickness, gives

$$\frac{\tilde{\delta}}{\Delta} = \frac{\kappa}{\Pi + 1}. \tag{27}$$

This shows that $\Pi$ is constant for the zero pressure gradient boundary layer, if indeed $\Delta$ is the proper length scale in the outer layer. For small $y/\tilde{\delta}$, the defect law (26) must approach the logarithmic shape (15). This gives

$$C' = \frac{1}{\kappa}\left(\ln\left(\frac{\kappa}{\Pi + 1}\right) + 2\Pi\right). \tag{28}$$

## 3. Convergence to the similarity scalings

The boundary-layer equations were solved for the turbulence models, using Spalart's DNS at $\mathrm{Re}_\theta = 300$ as a starting condition. The influence of the initial profile is restricted to about $\mathrm{Re}_\theta = 1000$; this was checked by increasing and decreasing the turbulence velocity and length scales in the initial profile at $\mathrm{Re}_\theta = 300$ by a factor 5. Independent of the initial conditions, all tested models turn out to converge to the classical similarity scalings, in the inner and outer layer, for increasing Reynolds number.

Fig. 1 shows the streamwise velocity and the turbulence quantities in the inner layer for different $\mathrm{Re}_\theta$ values, as obtained with the differential Reynolds-stress model. Also two relatively low Reynolds numbers are included, namely $\mathrm{Re}_\theta = 670$ and 1410, for which DNS exist as well. At these low values the logarithmic part of the wall function is still small, but it is extended to the range in between $y^+ = 100$ and $10^7$ for $\mathrm{Re}_\theta = 5.4 \times 10^7$. The values $\overline{-u'v'}^+ = 1$ and $k^+ = 1/c_\mu^{1/2}$ in the inertial sublayer (see Eq. (20)) are first reached for $\mathrm{Re}_\theta$ slightly above $10^4$. It is remarkable that the wall function for the turbulent dissipation rate is established very quickly; even for Reynolds numbers below 1000 the inertial sublayer already gives $\epsilon = 1/\kappa y^+$.

To monitor the convergence to the similarity scalings in the outer layer, Fig. 2 shows different characteristic quantities (obtained for the $k$–$\epsilon$ model, but the other models show almost the

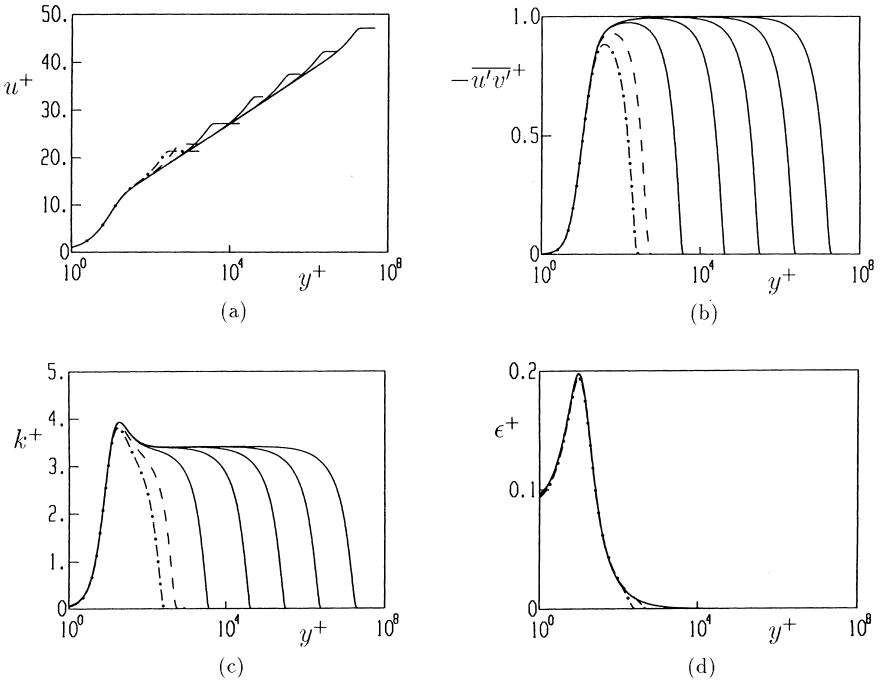


Fig. 1. Appearance of the law-of-the-wall for increasing Reynolds number according to the differential Reynolds-stress model; (a) velocity, (b) Reynolds shear stress, (c) turbulent kinetic energy, (d) turbulent dissipation rate. $\mathrm{Re}_\theta$ is 670 (–·–), 1410 (– –), $10^4$, $1.2 \times 10^5$, $8.8 \times 10^5$, $6.8 \times 10^6$ and $5.4 \times 10^7$.

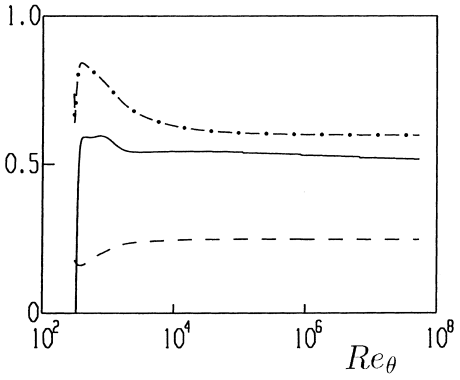


Fig. 2. Convergence to the similarity state of different characteristic parameters ($k$–$\epsilon$ model); —— $\Pi$; – – – $10 \times v_{t,\max}/U\delta^*$; –·– $\frac{1}{10} \times G$.

same convergence behaviour): Coles' wake-strength parameter $\Pi$, Clauser's wake parameter $G$, and the scaled maximum turbulent viscosity $v_{t\max}/U\delta^*$. The Clauser parameter gives the slowest convergence to its final constant value. All parameters are almost converged at $\mathrm{Re}_\theta = 10^4$, which is in fair agreement with the evaluation of experiments by Dussauge et al. (1996), showing that similarity is obtained at about $\mathrm{Re}_\theta = 5000$. The convergence to the similarity profile in the outer layer for the velocity and turbulence quantities is shown in Fig. 3, as obtained for the differential Reynolds-stress model for increasing Reynolds number. The profiles coincide, up to graphical accuracy, for $\mathrm{Re}_\theta = 10^4$ and larger. For the velocity and the turbulent dissipation rate, even the profiles for $\mathrm{Re}_\theta = 670$ and 1410 are already close to their similarity shape.

Table 1 gives some numerical values for different quantities in the inner and outer layer, as obtained with the $k$–$\epsilon$ model up to $\mathrm{Re}_x = 10^{11}$. The turbulence quantities in the inner layer $(\overline{u'v'}_{\max}, k^+_{\max})$ and in the outer layer $(v_{t,\max}/U\delta^*)$ have reached their asymptotic values up to at least 3 or 4 significant digits. The table also shows that the boundary layer thickness $\delta_{95}$ (defined as the $y$ position where the streamwise velocity is 95% of its free-stream value), which is often used to present velocity profiles, is not a proper length scale: $\delta_{95}/\Delta$ shows an, albeit small, decay for increasing Reynolds number.

Furthermore the table shows that the wall-shear stress coefficient $c_f$ (which equals $2(u_\tau/U)^2$), converges to zero for increasing Reynolds number. The shape factor $H$ slowly decreases to 1. Even at the largest considered Reynolds number ($\mathrm{Re}_x = 10^{11}$), however, the shape factor is 1.145, which is still significantly above its asymptotic value. Fig. 4 compares the wall-shear stress coefficient and the shape factor according to the different turbulence models with experimental data. All models closely agree with the experiments, except for the algebraic model which slightly overpredicts the shape factor. In the figure showing the wall-shear stress also the semi-empirical curve due to Fernholz (1971) and Fernholz and Finley (1996) is shown as a solid line. The curve is based on Eq. (16); $\mathrm{Re}_{\delta^*}$ is replaced by $\mathrm{Re}_\theta$ (approximating $H$ by 1), and the constants are taken as $(C + C') = 5.05$ and $\kappa = 0.4$.

We have examined how the coefficients $\alpha$, $\omega$, $\gamma$ and $\chi$, as computed with the boundary-layer equations using the Launder and Sharma $k$–$\epsilon$ model, behave for large Reynolds numbers: the leading-order term (being an integer power of $u_\tau/U$) in the deviation from the limiting values agrees with the series expansion (17). We also checked that the profiles for the velocity and turbulence quantities as obtained from the defect-layer equation (being of course independent of the Reynolds number) are indeed very close to the profiles obtained from the boundary-layer equations at $\mathrm{Re}_x = 10^{11}$. This all proves that the solution of the turbulent boundary-layer equations for a flat plate under zero pressure gradient at large Reynolds number is equal to the similarity solution described by the defect-layer equation (18).

Table 1
Asymptotic behaviour of the Launder and Sharma $k$–$\epsilon$ model

| $Re_x$ | $Re_\theta$ | $c_f$ | $H$ | $\delta_{95}/\Delta$ | $\overline{-u'v'}_{max}/u_\tau^2$ | $k_{max}/u_\tau^2$ | $\nu_{t,max}/U\delta^*$ |
|---|---|---|---|---|---|---|---|
| $1.88 \times 10^6$ | 1410 | 0.00360 | 1.433 | 0.196 | 0.922 | 3.313 | 0.0223 |
| $10^7$ | $1.27 \times 10^4$ | 0.00248 | 1.282 | 0.199 | 0.976 | 3.348 | 0.0246 |
| $10^8$ | $1.03 \times 10^5$ | 0.00182 | 1.223 | 0.190 | 0.992 | 3.352 | 0.0249 |
| $10^9$ | $7.88 \times 10^5$ | 0.00140 | 1.189 | 0.180 | 0.997 | 3.352 | 0.0249 |
| $10^{10}$ | $6.16 \times 10^6$ | 0.00111 | 1.164 | 0.169 | 0.999 | 3.352 | 0.0248 |
| $10^{11}$ | $4.93 \times 10^7$ | 0.00090 | 1.145 | 0.159 | 1.000 | 3.352 | 0.0248 |

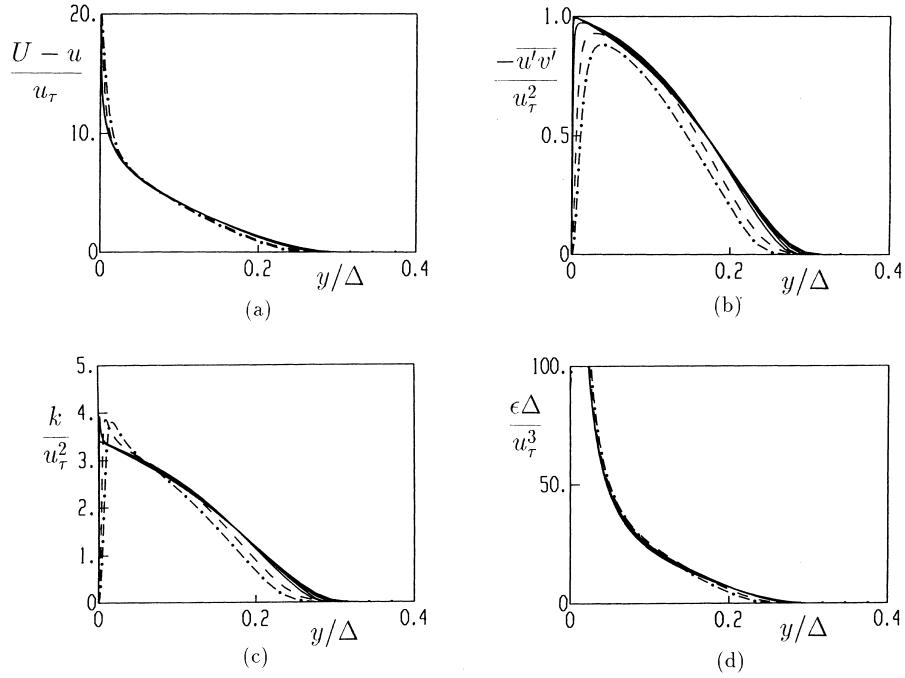


Fig. 3. Appearance of the defect law for increasing Reynolds number according to the differential Reynolds-stress model; (a) velocity, (b) Reynolds shear stress, (c) turbulent kinetic energy, (d) turbulent dissipation rate. $Re_\theta$ is 670 (–·–), 1410 (– –), $10^4$, $1.2 \times 10^5$, $8.8 \times 10^5$, $6.8 \times 10^6$ and $5.4 \times 10^7$.

## 4. Comparison with experiments and DNS

In this section the similarity solutions in the inner layer and outer layer according to the different turbulence models will be compared with each other. The solutions are also compared with DNS and experiments, available in the literature.

Fig. 5 compares the velocity and turbulent kinetic energy in the inner layer (a and b) and the outer layer (c and d), as computed at about $Re_\theta = 5 \times 10^7$ with the algebraic model, the $k$–$\epsilon$ model, the $k$–$\omega$ model, and the differential Reynolds-stress model, respectively. The Reynolds number is so large that the curves almost coincide with the similarity solution. All models reproduce almost the same logarithmic wall function, which is very close to the generally accepted best fit to the experiments (denoted as a dashed line): $u^+ = (1/\kappa)\ \ln\ y^+ + C$, with $\kappa = 0.41$, $C = 5$. For the velocity in the outer layer the solutions of all models almost coincide, except for the algebraic model, which predicts a too thin boundary layer. Considerable differences between the models are found for the turbulent kinetic energy in the viscous sublayer and the buffer layer, whereas there is close agreement in the inertial sublayer and in the outer layer. Most remarkable is the occurrence of a peak in the turbulent kinetic energy in the buffer layer, for the $k$–$\omega$ model and the differential Reynolds-stress model, which is absent for the Launder and Sharma $k$–$\epsilon$ model.

Fig. 6(a) compares the wall function in the inner layer for the turbulent kinetic energy according to the differential Reynolds-stress model with DNS at $Re_\theta = 670$ and 1410. Also the DNS show a peak for the kinetic energy in the buffer layer, which is even larger than predicted by the DRSM. It is noted that the Reynolds number in the DNS is still too small for the expected constant level of the kinetic energy in the inertial sublayer to have appeared; the law-of-the-wall has only been established up to about $y^+ = 100$, because the DNS for $Re_\theta = 670$ and 1410 coincide up to here. As shown in Fig. 6(b), a peak is also found for both the DRSM, DNS and experiments in the buffer layer for the Reynolds normal stress $\overline{u'u'}$. For this quantity as well, the peak in the DRSM is somewhat below the peak in the DNS and the experiments. It is remarkable that the experiments of Fernholz et al. (1995) in Fig. 6(b) reveal the formation of a second peak in the inertial sublayer for increasing Reynolds number. The formation of the second peak is also found in the experiments for the Reynolds normal stresses $\overline{v'v'}$ and $\overline{w'w'}$, and consequently also for the turbulent kinetic energy. None of the turbulence models predicts the second peak (in the kinetic energy or the Reynolds normal stresses), but instead they predict a constant level in the inertial sublayer. Nondimensionalization of the experimental value of the second-peak with the velocity scale $u_\tau$ does not lead to a Reynolds-number independent quantity.

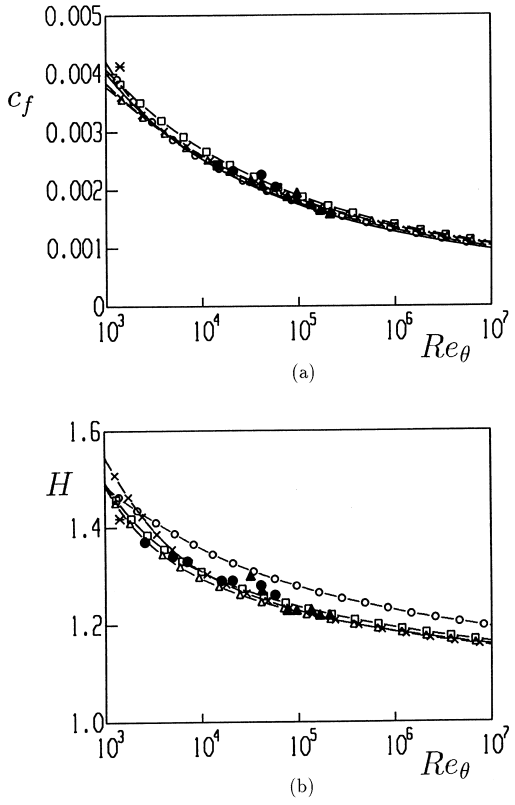


Fig. 4. Wall-shear stress coefficient (a) and shape factor (b) for increasing Reynolds number; models: ○–○ algebraic; △–△ $k$–$\epsilon$; ×–× $k$–$\omega$; □–□ DRSM. DNS: * Spalart (1988). Experiments: ▲ Winter and Gaudet (1973); ● Fernholz et al. (1995).

This shows that the second peak does neither follow the inner-layer scalings, nor the outer-layer scalings. More attention should be paid in future studies (experiments, DNS, turbulence modelling) to the existence and origin of the second peak.

Fig. 7 compares the outer layer according to the differential Reynolds-stress model with DNS and experiments of Fernholz et al. (1995). There is very good agreement for the streamwise velocity profile (Fig. 7(a)). Also the agreement for the Reynolds shear stress (Fig. 7(b)) is quite good, although the thickness of the boundary layer in the experiments is slightly smaller than in the DNS, whereas the DRSM gives a thickness just in between the experiments and the DNS. The agreement for the turbulent kinetic energy (Fig. 7(c)) and the Reynolds normal stress $\overline{u'u'}$ (Fig. 7(d)) is only good for $y/\Delta$ above about 0.05. For smaller $y/\Delta$ values the experiments show the second-peak (which seems to scale with the length scale $\Delta$, but not with the velocity scale $u_\tau$), whereas the DNS shows the first peak. The first peak in the DNS is in fact part of the inner layer, but it is visible in the figure because of the relatively low Reynolds number. The prediction with the DRSM for the Reynolds normal stress $\overline{v'v'}$ (Fig. 7(e)) is slightly below the experiments and the DNS, whereas the agreement for $\overline{w'w'}$ is good for the whole outer layer.

Table 2 compares the numerical values of different quantities in the inner and outer layer as obtained at large Reynolds numbers from experiments and turbulence models. Also included are DNS values at somewhat lower Reynolds numbers. There is close agreement for the constants $\kappa$ and $C$ in the logarithmic wall function for the velocity. In the outer layer there is good agreement for the Clauser parameter $G$ and for the scaled maximum turbulent viscosity, $\nu_{t,\max}/U\delta^*$. With respect to the latter quantity, only the Cebeci and Smith model finds a value that is about 35% below the DNS and the prediction of the other turbulence models. Differences are largest for the wake-strength parameter $\Pi$ and for the parameter $\Delta^*$, as introduced by Coles (1956). The latter parameter is defined as the maximum difference between the defect law and the log-

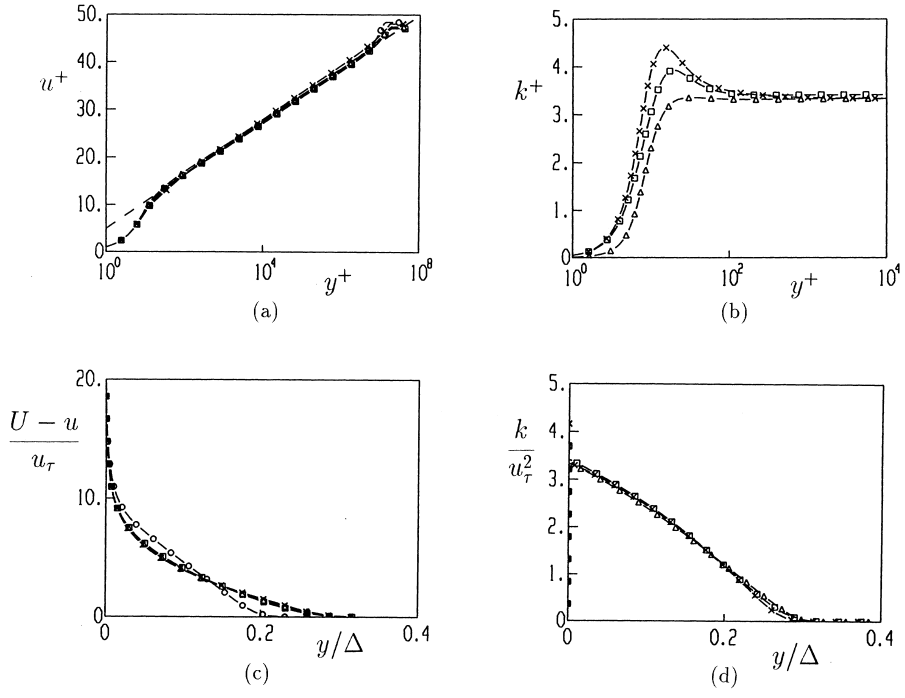


Fig. 5. Comparison between turbulence models at $\mathrm{Re}_\theta \approx 5.4 \times 10^7$; (a) velocity in inner layer (dashed line is $u^+ = (1/\kappa)\ \ln\ y^+ + C$, with experimental values $k = 0.41$, $C = 5$); (b) kinetic energy in inner layer; (c) velocity in outer layer; (d) kinetic energy in outer layer; models: ○–○ algebraic; △–△ $k$–$\epsilon$; ×–× $k$–$\omega$; □–□ DRSM.

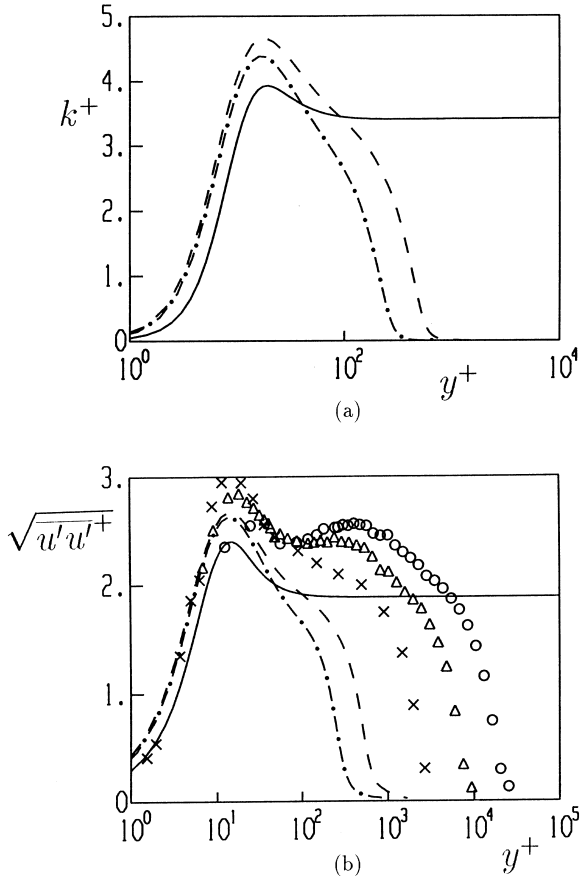


Fig. 6. Comparison of the differential Reynolds-stress model with experiments and Direct Numerical Simulations in the inner layer; (a) turbulent kinetic energy, (b) Reynolds normal stress $\overline{u'u'}$; —— DRSM at $Re_\theta = 5.4 \times 10^7$; experiments by Fernholz et al. (1995): $\times$ $Re_\theta = 7140$, $\triangle$ $Re_\theta = 20920$, $\circ$ $Re_\theta = 57720$; DNS by Spalart (1988): –·– $Re_\theta = 670$; - - - $Re_\theta = 1410$.

arithmic wall function for the scaled velocity $u/U_\tau$. Combining Coles' expression for the defect law (25) at $y = \tilde{\delta}$ with the wall function (14) gives

$$\Delta^* = \frac{2\Pi}{\kappa}. \tag{29}$$

This relation is not exactly satisfied in Table 2, because we determined $\Pi$ from Eq. (25) (setting $y = \tilde{\delta}$), after elimination of $\tilde{\delta}$ by using the *approximating* equation (27). This procedure also proves that $\Pi$, and consequently $\Delta^*$, are very sensitive to changes in the wall shear stress; in fact a change in $u_\tau/U$ leads to a change in $\Pi$ that has been amplified with the large factor

$$\left(\frac{U}{u_\tau}\right)^2 \Big/ \left(\frac{1}{\kappa}\frac{1}{\Pi + 1} - \frac{2}{\kappa}\right).$$

This shows that $\Pi$ is not a very good parameter to indicate the state of the boundary layer. In this respect $G$ is a much more robust indicator.

## 5. Conclusions

Numerically accurate solutions were obtained for the turbulent boundary-layer equations, describing the incompressible boundary layer along a plate under zero pressure gradient. Monitoring characteristic quantities (such as the Clauser parameter $G$) shows that the large-Reynolds-number state is established at about $Re_\theta = 10^4$, which is in good agreement with the value of 5000 reported in experiments.

All four tested models (an algebraic, $k$–$\epsilon$, $k$–$\omega$, and a differential Reynolds stress model) reproduce the classical similarity scalings, that are the velocity scale $u_\tau$ and the length scale $\nu/u_\tau$ in the inner layer (which defines the law-of-the-wall) and the velocity scale $u_\tau$ and the length scale $\delta^* U/u_\tau$ in the outer layer (which defines the defect law). The solution of the boundary-layer equations in the outer layer converges to the solution of the defect-layer equation proposed by Tennekes and Lumley (1972) and by Wilcox (1993). This was shown by numerically solving this defect-layer equation as well, and by monitoring the large-Reynolds-number behaviour of the coefficients appearing in the boundary layer equations, after transformation into outer-layer coordinates.

All the turbulence models give practically the same logarithmic wall function for the velocity in the inner layer, which is not surprising as some of the constants in the models were originally tuned to reproduce this profile. Differences between the models do occur, however, for the turbulence quantities in the inner layer, such as for the maximum of the turbulent kinetic energy in the buffer layer. The constants in the models were not explicitly tuned to reproduce the defect law in the outer layer, which thus is an important feature for their validation. The models give almost the same profile for the velocity and the turbulence in the outer layer, except for the algebraic model, which gives a too small boundary-layer thickness.

The derived similarity scalings and profiles were compared with Direct Numerical Simulations obtained by Spalart (1988) and with experiments, including the new data obtained by Fernholz et al. (1995). All considered turbulence models, except for the algebraic model, give good agreement. One point of difference is the second maximum in the turbulent kinetic energy, that is found to develop in the experiments for increasing Reynolds number. None of the models predicts

Table 2
Some quantities at large Reynolds number

| Model | $\kappa$ | C | $\Pi$ | $\Delta^*$ | $G$ | $\nu_{t,\max}/U\delta^*$ |
|---|---|---|---|---|---|---|
| Experiments | $\approx 0.41$ | $\approx 5.0$ | 0.4–0.6 | 2–2.5 | $\approx 6.5$ | – |
| DNS $Re_\theta = 670$ | $\approx 0.38$ | $\approx 4.3$ | 0.25 | $\approx 1.2$ | 6.6 | 0.0257 |
| DNS $Re_\theta = 1410$ | $\approx 0.40$ | $\approx 4.7$ | 0.24 | $\approx 1.4$ | 6.5 | 0.0258 |
| Algebraic model | 0.415 | 5.3 | 0.67 | 3.6 | 7.3 | 0.0169 |
| $k$–$\epsilon$ model | 0.431 | 6.4 | 0.52 | 2.3 | 6.0 | 0.0248 |
| $k$–$\omega$ model | 0.406 | 5.3 | 0.32 | 1.8 | 6.0 | 0.0264 |
| DRSM | 0.422 | 5.4 | 0.44 | 2.0 | 6.1 | 0.0252 |

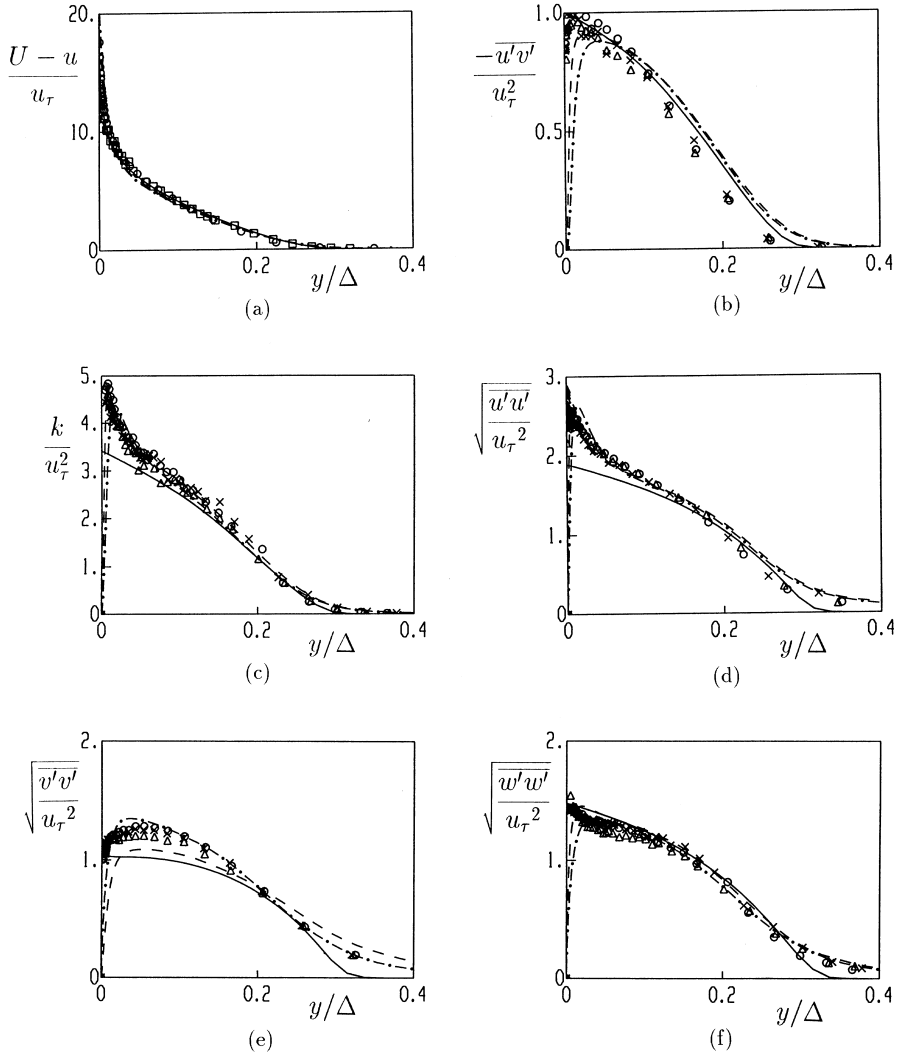


Fig. 7. Comparison of the differential Reynolds-stress model with experiments and Direct Numerical Simulations in the outer layer; (a) velocity; (b) Reynolds shear stress, (c) turbulent kinetic energy, (d) Reynolds normal stress $\overline{u'u'}$; (e) Reynolds normal stress $\overline{v'v'}$; (f) Reynolds normal stress $\overline{w'w'}$; —— DRSM at $Re_\theta = 5.4 \times 10^7$; experiments by Fernholz et al. (1995): △ $Re_\theta \approx 2 \times 10^4$, × $Re_\theta \approx 4 \times 10^4$, ○ $Re_\theta \approx 6 \times 10^6$; experiments by Winter and Gaudet (1973)): □ $Re_\theta = 2.1 \times 10^5$; DNS by Spalart (1988): –·– $Re_\theta = 670$, - - - $Re_\theta = 1410$.

this feature. More attention should be paid to this second maximum in future studies.

## Acknowledgements

The author wishes to thank Professor H.H. Fernholz for kindly providing his recent experimental data.

## References

Barenblatt, G.I., 1993. Scaling laws for fully developed turbulent shear flows. Part 1. Basic hypotheses and analysis. J. Fluid Mech. 248, 513–520.

Cebeci, T., Smith, A.M.O., 1974. Analysis of Turbulent Boundary Layers. Academic Press, New York.

Clauser, F.H., 1954. Turbulent boundary layers in adverse pressure gradients. J. Aero. Sci. 21, 91–108.

Coles, D., 1956. The law of the wake in the turbulent boundary layer. J. Fluid Mech. 1, 191–226.

Dussauge, J.P., Smith, R.W., Smits, A.J., Fernholz, H., Finley, P.J., Spina, E.F., 1996. Turbulent boundary layers in subsonic and supersonic flow. Agardograph 335.

Fernholz, H.H., 1971. Ein halbempirisches Gesetz für due Wandreibung in kompressiblen turbulenten Grenzschichten bei isothermer und adiabater Wand. ZAMM 51, 146–147.

Fernholz, H.H., Finley, P.J., 1996. The incompressible zero-pressure-gradient turbulent boundary layer: An assessment of the data. Prog. Aerospace Sci. 32, 245–311.

Fernholz, H.H., Krause, E., Nockemann, M., Schober, M., 1995. Comparative measurements in the canonical boundary layer at $Re_{\delta 2} \leqslant 6 \times 10^4$ on the wall of the DNW. Phys. Fluids A 7, 1275–1281.

George, W.K., Knecht, P., Castillo, L., 1992. The zero-pressure gradient boundary layer revisited. In: Reed, X.B. (Ed.), Proceedings of Thirteenth Symposium on Turbulence, Rolla, Mo, USA.

Hanjalić, K., Jakirlić, S., Hadžić, I., 1995. Computation of oscillating turbulent flows at transitional Re-numbers. In: Durst, F. et al. (Eds.), Turbulent Shear Flows 9. Springer, Berlin, pp. 323–342.

Henkes, R.A.W.M., 1990. Natural-Convection Boundary Layers. Ph.D. Thesis, Delft University of Technology.

Henkes, R.A.W.M., 1997. Comparison of turbulence models for attached boundary layers relevant to aeronautics. Appl. Sci. Res. 57, 43–65.

Jakirlić, S., Hadžić, I., Hanjalić, K., 1994. Computation of non-equilibrium and separating flows at transitional and high Re-numbers with a new low-Re-number second-moment closure model. In: Proceedings of Strömungen mit Ablösung, AGSTAB, DGLR Congress, Erlangen, Germany.

Launder, B.E., Sharma, B.I., 1974. Application of the energy-dissipation model of turbulence to the calculation of flow near a spinning disk. Lett. Heat Mass Transfer 1, 131–138.

Millikan, C.B., 1938. A critical discussion of turbulent flows in channels and circular tubes. In: Dentalartog, J.P., Peters, H. (Eds.), Proceedings of Fifth International Congr. of Appl. Mech., Cambridge, pp. 386–392.

Rotta, J.C., 1950. Über die Theorie der turbulenten Grenzschichten. Mitt. aus dem Max-Planck Inst. für Strömungsforschung, 1; also translated as: On the theory of the turbulent boundary layer. NACA TM 1344, 1953.

Spalart, P.R., 1988. Direct numerical simulations of a turbulent boundary layer up to $Re_\theta = 1410$. J. Fluid Mech. 187, 61–98.

Tennekes, H., Lumley, J.L., 1972. A First Course in Turbulence. MIT Press, Cambridge, MA.

Townsend, A.A., 1976. The Structure of Turbulent Shear Flow. Cambridge University Press, Cambridge.

Von Kármán, T., 1930. Mechanische Ähnlichkeit und Turbulenz. Nachrichten der Konigliche Gesellschaft der Wissenschaften zu Göttingen, Math. Phys. Klasse, pp. 58–76.

Wilcox, D.C., 1993. Turbulence Modelling. DCW Industries Inc.

Winter, K.G., Gaudet, L., 1973. Turbulent boundary-layer studies at high Reynolds numbers at Mach numbers between 0.2 and 2.8. ARC R and M 3712.